Project information

Project full title	EuroSea: Improving and Integrating European Ocean Observing and Forecasting Systems for Sustainable use of the Oceans
Project acronym	EuroSea
Grant agreement number	862626
Project start date and duration	1 November 2019, 50 months
Project website	https://www.eurosea.eu

Deliverable information

Deliverable number	D7.6
Deliverable title	**Integration of in situ and satellite multi-platform data (estimation of carbon flux for trop. Atlantic)**
Description	Quantification of improvements in carbon flux data for the tropical Atlantic based on the multi-platform and neural network approach
Work Package number	WP7
Work Package title	Ocean climate indicators demonstrator
Lead beneficiary	Sarbonne Universite (SU)
Lead authors	Marine Fourrier
Contributors	Hervé Claustre, Laurent Coppola, Björn Fiedler, Cathy Wimart-Rousseau
Due date	28 February 2023
Submission date	13 March 2023
Comments	

This project has received funding from the European Union's Horizon 2020 research and innovation programme under grant agreement No. 862626.

https://doi.org/10.3289/eurosea_d7.6

Table of contents

Executive summary

This report presents the results of task 7.3 on "Quantification of improvements in carbon flux data for the tropical Atlantic based on the multi-platform and neural network approach". To better constrain changes in the ocean's capture and sequestration of CO2 emitted by human activities, in situ measurements are needed. Tropical regions are considered to be mostly sources of CO_2 to the atmosphere due to specific circulation features, with large interannual variability mainly controlled by physical drivers (Padin et al., 2010). The tropical Atlantic is the second largest source, after the tropical Pacific, of CO_2 to the atmosphere (Landschützer et al., 2014). However, it is not a homogeneous zone, as it is affected by many physical and biogeochemical processes that vary on many time scales and affect surrounding areas (Foltz et al., 2019). The Tropical Atlantic Observing System (TAOS) has progressed substantially over the past two decades. Still, many challenges and uncertainties remain to require further studies into the area's role in terms of carbon fluxes (Foltz et al., 2019). Monitoring and sustained observations of surface oceanic CO_2 are critical for understanding the fate of CO_2 as it penetrates the ocean and during its sequestration at depth.

This deliverable relies on different observing platforms deployed specifically as part of the EuroSea project (a Saildrone, and 5 pH-equipped BGC-Argo floats) as well as on the platforms as part of the TAOS (CO_2-equipped moorings, cruises, models, and data products). It also builds on the work done in D7.1 and D7.2 on the deployment and quality control of pH-equipped BGC-Argo floats and Saildrone data. Indeed, high-quality homogeneously calibrated carbonate variable measurements are mandatory to be able to compute air-sea CO_2 fluxes at a basin scale from multiple observing platforms.

1. Introduction

The global ocean plays a crucial role in regulating the ocean's climate. Specifically, the ocean takes up about ~25% of anthropogenic CO_2, absorbing an estimated 525 billion tons of CO_2 since the industrial era (von Schuckmann et al., 2022). The ocean carbon sink has increased over the past 30 years at a pace of 0.06 ± 0.09 PgC/year. However, uncertainties in the estimates are largely due to a lack of observations. To improve our understanding of the ocean's role in global changes and assess long-term trends in the uptake and storage of CO_2, sustained high-quality measurements are needed. One area of the global ocean that remains poorly constrained in terms of its response to CO_2 is the tropical Atlantic.

Tropical regions are considered to be mostly sources of CO_2 to the atmosphere due to specific circulation features, mainly through upwelling processes, bringing CO_2-rich waters from the deep ocean to the surface where outgassing occurs due to high temperatures, with large interannual variability largely controlled by physical drivers (Padin et al., 2010). The tropical Atlantic is the second largest source, after the tropical Pacific, of CO_2 to the atmosphere, releasing about 0.10 Pg C yr^{-1} (Landschützer et al., 2014). However, it is not a homogeneous zone, including for example oxygen minimum areas along the African coasts; the equatorial cold tongue along Guinea contrasting with warm nutrient-rich outflows of the Amazonian River. The Tropical Atlantic is affected by multiple physical and biogeochemical processes, varying on many time scales, and impacting surrounding areas (Foltz et al., 2019). For example, because of its connection to the Atlantic Meridional Overturning Circulation (AMOC; Boers, 2021), changes in this region of the ocean have global consequences. In this contrasted area, short time series and high natural variability prevent clear carbon trends from emerging, though there are indications of decadal variations with large implications for anthropogenic CO_2 uptake (Park and Wanninkhof, 2012). Furthermore, this area is known to exhibit significant interannual variability of air-sea CO_2 fluxes closely linked to climate variability (Lefèvre et al., 2013; Ibánhez et al., 2017). The Tropical Atlantic Observing System (TAOS) has progressed substantially over the past two decades (Speich et al., 2019). Still, many challenges and uncertainties remain requiring further studies into the area's role in terms of carbon fluxes (Foltz et al., 2019). Monitoring and sustained observations of surface oceanic CO_2 are critical for understanding the fate of CO_2 as it penetrates the ocean and during its sequestration at depth.

This deliverable takes advantage of the Saildrone and pH-equipped BGC-Argo floats deployed in the frame of the EuroSea project in the area. It also relies on existing moorings equipped with pCO_2 sensors, cruises, models, and data products focusing on the carbonate system in the ocean.

In the framework of EuroSea, the aim of this deliverable is, to use a combination of multi-platform observations, models, and neural network techniques, to assess our ability to derive air-sea CO_2 fluxes in the tropical Atlantic region over the last five years (as few data are available for 2022 and 2023, the selected period is 2018-2021). This deliverable relies on the work done in EuroSea D7.1 and D7.2 which describe the observing platforms deployed in the tropical Atlantic in the EuroSea project (specifically Saildrone and BGC-Argo floats) and the correction of their data to ensure good quality observations.

2. Datasets and methods

2.1. In situ carbon datasets

Observing platforms

Numerous datasets acquired through various observing platforms have been used in this study (Figure 1A).

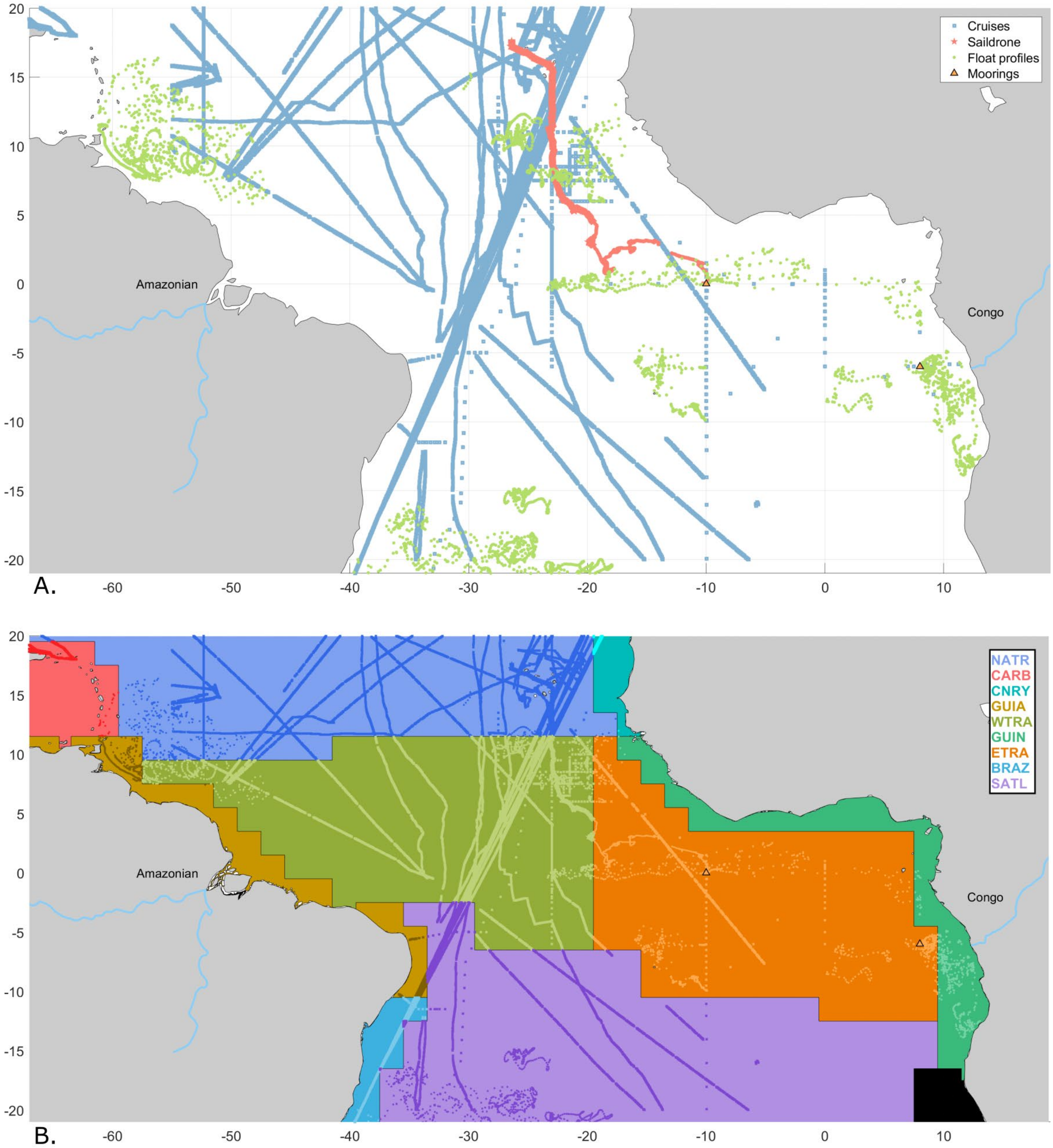

Figure 1. Map of the tropical Atlantic (A) showing the in situ data used in this study (cruises (blue squares, Saildrone (red stars), Argo float profiles (green dots) and moorings (orange triangles) and (B) showing Longhurst's (2007) biogeochemical provinces (BGCPs) over the in situ data. The BGCPs acronyms are the following: NATR (grey blue), CARB (red), CNRY (cyan), GUIA (brown), WTRA (olive), GUIN (green), ETRA (orange), BRAZ (blue), and SATL (purple).

A Saildrone (SD, red stars in Figure 1A) platform equipped with an ASVCO2 system (PMEL, NOAA) has been deployed in the EuroSea mission operating area and recorded data between September 18th, 2021, and March 8th, 2022 (see D7.1 (Fiedler et al., 2022) and D7.2 (Wimart-Rousseau et al., 2022) for more details). Once the SD was recovered, raw data were downloaded and processed following the procedure described in Sutton et al., (2014). The SD measured wind speed at 5 meters above the sea surface, xCO_2 in the atmosphere together with subsurface xCO_2, temperature, salinity, and dissolved oxygen (O_2).

Five BGC-Argo floats (WMOS 6903874 to 6903878) equipped with pH and O_2 sensors were deployed in the tropical Atlantic in 2021. Out of the five floats, one's pH sensor malfunctioned and was remotely turned off to preserve the battery. The four other floats continued cycling and are still acquiring data to this day. In D7.2 and following Argo Delayed Mode Quality Control procedures adapted to the float's sampling specificities, pH from the Argo floats was quality controlled and corrected for sensor drift. Furthermore, 28 O_2-equipped BGC-Argo floats in total have sampled the tropical Atlantic (green dots in Figure 1A).

A collection of data products (blue squares in Figure 1A) pertaining to the measurement of ocean carbon variables was used. First, the 2022 update from the Surface Ocean CO_2 Atlas (SOCAT, Bakker et al., 2016), a synthesis of quality-controlled CO_2 values for the global surface oceans and coastal seas with direct pCO_{2sw} (pCO_2 in seawater) values. Second, the 2022 update of the Global Ocean Data Analysis Project (GLODAPv2.2022, Olsen et al., 2016; Lauvset et al., 2022), a synthesis effort providing compilations of numerous surface-to-bottom ocean biogeochemical data determined through chemical analysis of water samples. In terms of the carbonate system, the variables recorded in GLODAP are total alkalinity (A_T) and total dissolved inorganic carbon (C_T), and seawater pH on the total scale at both 25 °C and *in situ* temperature (pH_T). Third, data were acquired in the frame of the SOOP (Ship Of Opportunity Program; Goni et al., 2010) which records data from volunteer merchant ships regularly crossing the area. Parts of the Atlantic SOOP network are operated in the European Research Infrastructure 'Integrated Carbon Observation System' (ICOS) and the 'Surface Ocean CO_2 Reference Observing Network' (SOCONET). Specifically, the France-Brazil SOOP line has been making underway carbonate chemistry measurements since July 2014 (PI. Nathalie Lefèvre at LOCEAN/IPSL in France). Specifically, pCO_2sw surface measurements are performed between Le Havre, France, and Santos, Brazil (Watson et al., 2018). Fourth, we used the Lamont-Doherty database (LDEO, Takahashi et al., 2019) containing global ocean surface pCO_{2sw} from 1957 to 2019 assembling high-quality reprocessed pCO_2 data obtained using the equilibrator-analyser method. Finally, annual oceanographic PIRATA cruises are conducted and performed to ensure the maintenance of the PIRATA mooring network but also to perform conductivity-temperature-depth (CTD) casts and *in situ* biogeochemical parameters measurements. Between March and April 2021, the PIRATAFR31 cruise sampled surface and water column measurements of A_T and C_T.

For GLODAP and PIRATAFR31, as no direct pCO_{2sw} measurement existed when A_T and C_T were available pCO_{2sw} was calculated using CO2SYSMATLABv2 (Lewis et al., 1998; van Heuven et al., 2011). Thermodynamic calculations within the carbonate system used the carbonic acid dissociation constants of Mehrbach et al. (1973) as refit by Dickson and Millero (1987), the dissociation constant for bisulfate of Perez & Fraga (1987) and Uppström (1974) for the ratio of total boron to salinity.

Since 2008, several deployments of CO_2 sensors have been carried out on four PIRATA moorings (Bourlès et al., 2018, 2019). Due to various technical issues but also due to vandalism, long-term CO_2 time series data are difficult to obtain. Since 2017, a mooring has been measuring the fugacity of CO_2 at 6°S 8°E in the PIRATA network (orange triangle in Figure 1A). The corresponding fCO_2 data are archived by SOCAT. The buoy at 6°S 8°E drifted in 2018 and again in 2019 (Lefèvre et al., 2021), therefore, this site was abandoned leaving us only with a limited time series. Since 2020 a mooring has been measuring the fugacity of CO_2 at 0°N 10W in the PIRATA network, however, its data is still being corrected and is not yet available in SOCAT.

Data products

In recent years, more and more models are now aiming to reproduce oceanic CO_2 to better study air-sea fluxes and the ocean carbon cycle. As *in situ* data can be scarce and lack spatiotemporal coverage, some model outputs were used as comparisons to the *in situ* observations used in this study.

A global gridded 1°x1° surface ocean pCO_2 product hereafter named **StepCO2** spanning from January 1992 to December 2020 and reconstructed using a stepwise regression algorithm and a feed-forward neural network (Zhong et al., 2021, 2022). It relies on varying predictors depending on the oceanic area among latitude, longitude, time, sea surface temperature (SST) and anomaly, sea surface salinity (SSS) and anomaly, sea surface height (SSH) and anomaly, Mixed Layer Depth (MLD) and anomaly, 10m wind speed, dry air mixing ratio of atmospheric CO_2 and anomaly, sea ice fraction, bathymetry, chlorophyll a, and anomaly, the velocity of ocean currents at 5m, 65m, 105m, and 195m, sea level pressure and surface pressure, climatologies of O_2, nitrate, phosphate, and silicate together with the oceanic El Niño Index (Huang et al., 2017) and the Southern Hemisphere Annular Mode Index (Marshall, 2003). When validating their algorithm and product with the SOCAT dataset and independent observations, Zhong et al., (2022) showed that using regional-specific predictors selected by the stepwise FFNN algorithm retrieved a lower predicting error than globally similar predictors. For the tropical Atlantic, ('south Atlantic' in the paper) they recovered pCO_{2sw} with Mean Absolute Error (MAE) and Root Mean Square Error (RMSE) of 11.32 and 17.99 µatm respectively.

The Global Ocean Surface Carbon Product (MULTIOBS_GLO_BIO_CARBON_SURFACE_REP_015_008, Chau et al., 2022), hereafter named **Carbonsurf** is a dataset delivered by the Copernicus Marine Environmental Monitoring service. It contains ocean carbon surface variables on a regular grid (1°x1°) with a monthly resolution from 1985 to December 2021. These variables contain pCO_{2sw}, A_T, C_T, pH, and saturation states for surface waters with respect to calcite and aragonite and surface ocean downward mass flux. pCO_{2sw} is obtained from an ensemble of feed-forward neural networks (CMEMS-LSCE-FFNNv2, Chau et al., 2022) trained on 100 subsampled datasets from SOCAT. As predictors, SSS, SST, SSH, mixed layer depth, atmospheric CO_2 mole fraction, chlorophyll, pCO_{2sw} climatology, latitude, and longitude are used. Over the global ocean, the MAE and RMSD for pCO_{2sw} were 11.99 and 19.32 µatm, respectively (Chau et al., 2022).

OceanSODA-ETHZ (Gregor and Gruber, 2021; Gregor, 2021), hereafter named **OceanSODA**, is a methodologically consistent global gridded data set of surface ocean carbon variables, namely A_T, C_T, pCO_{2sw}, pH, and the saturation state with respect to calcite at a monthly resolution over the period 1985 through 2021 at a spatial resolution of 1°x1°. This product was created by extrapolating in time and space pCO2sw from SOCAT and A_T from GLODAP using the newly developed Geospatial Random Cluster Ensemble Regression (GRaCER) method (Gregor and Gruber, 2021). This method is based on an ensemble of cluster regressions. For the open ocean, OceanSODA retrieves pCO_{2sw} with RMSE of 14 µatm.

2.2. Derived variables and miscellaneous data

Machine learning methods

Nowadays, machine learning methods such as neural networks are being used more and more for oceanographic applications to virtually densify the limited number of measurements that can be done by autonomous platforms. These methods allow for the prediction of carbonate system variables with a given accuracy, relying only on temperature, salinity, and O_2 together with the position in time and space. Specifically, carbonate system variables (A_T, C_T, pCO_{2sw}) were derived using the CONTENT (Bittig et al., 2018) neural-network-based method. This neural network method was selected as it ensures consistency between carbonate system variables when producing estimates. Therefore, while we cannot measure pCO_{2sw} directly from BGC-Argo floats, they can be derived using neural networks. Therefore, for the aforementioned pH-equipped BGC-Argo floats, pCO_{2sw} was derived through CO2SYS using the pH from the Argo float and A_T from CONTENT using the float's O_2, temperature, salinity, and pressure. To densify our dataset, we also applied the CONTENT neural networks to all O_2-equipped BGC-Argo floats in the tropical Atlantic to directly derive pCO_{2sw} (28 floats).

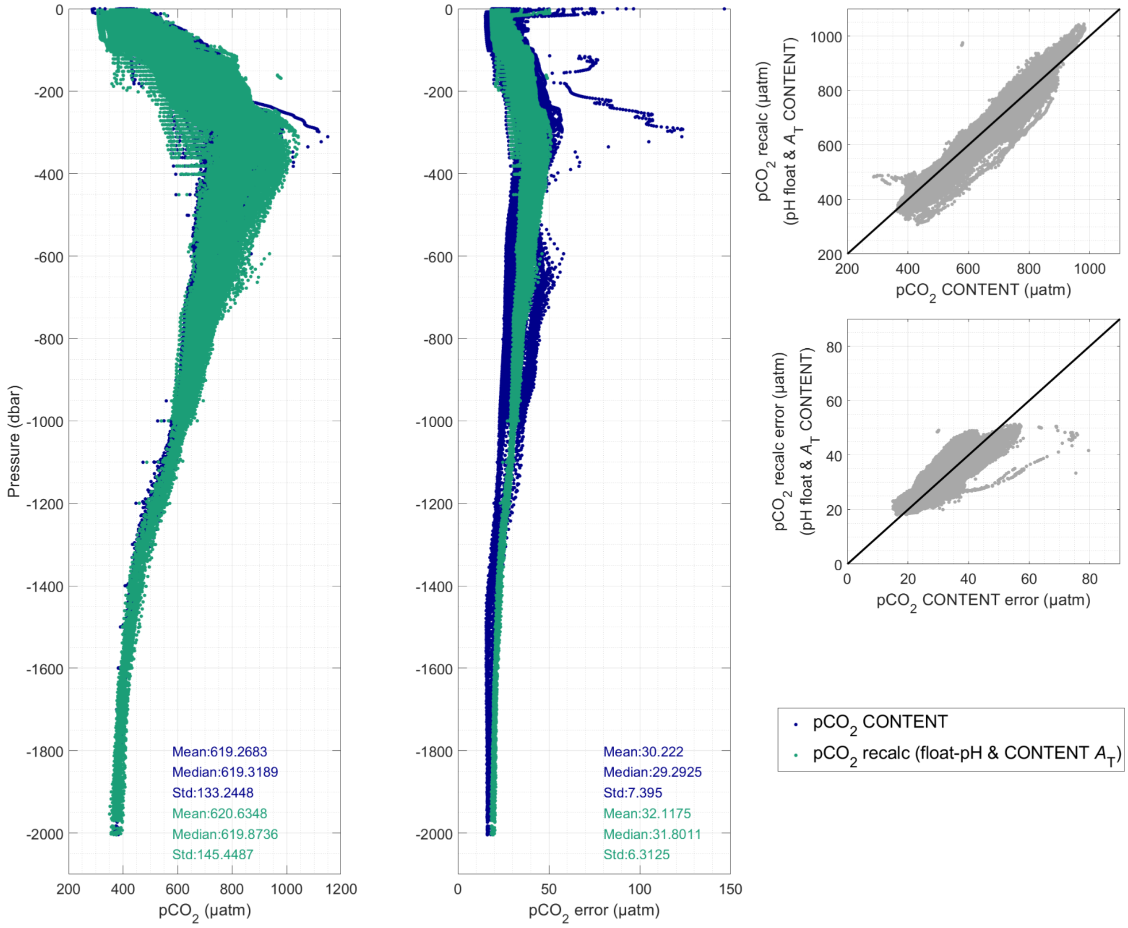

Figure 2. BGC-Argo pCO2sw profiles (A) and associated error (B) derived directly from CONTENT (dark blue) and derived from the float's pH and CONTENT's AT (green). Regressions between pCO2 (C) and pCO2 error (D) directly from CONTENT and recalculated. The black line represents the 1:1 regression. The mean, median, and standard deviation for CONTENT and recalculated pCO_{2sw} and pCO_{2sw} errors are written on panels A and B.

Differences between pCO_{2sw} predicted directly from CONTENT and pCO_2 derived from float-pH data and A_T from CONTENT are limited (less than 1 µatm in mean, Figure 2). The CONTENT neural network directly provides a local uncertainty that was used for pCO_{2sw}. However, pCO_{2sw} uncertainties for the recalculated pCO_{2sw} were computed using 'errors', a routine for uncertainty propagation for the marine carbon dioxide system (Orr et al., 2018) based on the A_T uncertainty provided by CONTENT and a pH uncertainty of 0.02 pH units (as calculated for EuroSea pH floats in D7.2). Errors for direct pCO_{2sw} estimates are lower than those when pCO_{2sw} is recalculated from the Argo float's pH, but the differences remain moderate (mean difference of 2 µatm). Therefore, while *in situ* pH measurements are essential, it appears that deriving oceanic pCO_2 data directly using a neural network method such as CONTENT can provide comparable results. However, in the specific case of EuroSea, pH sensors had a lot of issues among which drift which was corrected during delayed mode quality control procedures (details in D7.2, Maurer et al., 2021), largely increasing the pH uncertainty. Indeed, for the SOCCOM floats in the Southern Ocean, Johnson et al. (2017) showed that the correction of pH from Argo floats can lead, in some cases, to large amounts of high-quality pH data reaching accuracies of 0.005 pH units, much lower than ours. For the sake of comparison, we calculated a theoretical error propagation in case our pH error had reached 0.005 pH units rather than 0.02 pH units. This would have driven the pCO_{2sw} error estimate down to 8.50 ± 1.79 µatm. The deployment of pH sensors on Argo floats should thus be maintained, but while being careful of the sensor's quality before deployment. In cases where no pH sensor is available, good quality O_2 from BGC-Argo floats is enough to derive pCO_{2sw} from neural network techniques.

Normalized pCO_{2sw}

The seasonality of pCO_{2sw} is mainly controlled by SST. To minimize this effect between platforms and areas, pCO_{2sw} is normalized to a constant temperature (here 26°C, the average SST in the tropical Atlantic, hereafter named pCO_{2sw}@26C) using the method described by Takahashi et al, (1993), with the temperature sensitivity of CO_2 of γT = 4.23% per degree Celsius:

$$pCO_{2sw}@26C = pCO_{2sw} \times exp(\gamma T \times (26 - SST))$$

CO_2 fluxes

To be able to look at air-sea CO_2 fluxes rather than only surface pCO_{2sw}, atmospheric pCO_2 (pCO_{2atm}) is necessary. While the Saildrone measures atmospheric pCO_2, it is the only one of the observing platforms used in this study to do so. Therefore, we used the **SeaFlux** dataset (Fay et al., 2021), specifically the update for 2021 (personal communication Luke Gregor). This dataset provides a consistent approach specifically targeting the most commonly used atmospheric and oceanic pCO_2 data products to deliver an end-product for intercomparisons within assessment studies such as the Global Carbon Budget (Friedlingstein et al., 2022). Specifically, SeaFlux provides the air-sea CO_2 flux for different wind products (FCO_2), k_w the gas transfer velocity calculated for winds scaled independently to a 14-C bomb flux estimate of 16.5 cm/hr using the quadratic formulation by Wanninkhof (1992), pCO_{2sw} from various sources, the sea ice fraction from the OISST product, and pCO_{2atm} calculated from NOAA's marine boundary layer product with ERA5 mean sea level pressure corrected for pH_2O.

CO_2 fluxes (FCO_2, mmol $m^{-2}d^{-1}$) between the ocean and the atmosphere were computed using the CO2flux function from the CO2flux toolbox[1] following the equation of Wanninkhof (1992):

$$FCO_2 = k \times \alpha \times (pCO_{2sw} - pCO_{2atm})$$

where k is the gas transfer velocity for CO_2 (in $cm.h^{-1}$), α is the solubility coefficient of CO_2 (in mol L^{-1} atm^{-1}) calculated as a function of temperature and salinity following Weiss (1974), and pCO_{2sw} and pCO_{2atm} are the seawater and atmospheric partial pressure of CO_2 respectively (in µatm). By convention, a negative (positive) sign indicates a flux from the atmosphere to the ocean (from the ocean to the atmosphere).

The gas transfer velocities have been computed according to the equation proposed by Wanninkhof (1992):

$$k = 0.31 \times U_{10}{}^2 \times (\frac{Sc}{660})^{-1/2}$$

where U_{10} is the wind speed (in $m.s^{-1}$), and Sc is the Schmidt number (dimensionless) calculated according to the equation in Wanninkhof (1992).

In this study, pCO_{2atm} was obtained from the SeaFlux dataset and is the dry air mixing ratio of atmospheric CO_2 (xCO_2) from the ESRL surface marine boundary layer CO_2 product (Dlugokencky et al., 2019)[2] multiplied by ERA5 sea level pressure (Hersbach et al., 2020) at monthly resolution and applying the water vapor correction according to Dickson et al. (2007). The solubility coefficient α was computed using EN4 near-surface salinity (Good et al., 2013), NOAA Optimum Interpolation Sea Surface Temperature V2 (OISSTv2) (Reynolds et al., 2002), and European Centre for Medium-Range Weather Forecasts (ECMWF) ERA5 sea level pressure (Hersbach et al., 2020). The 10 m surface wind speed was obtained from the ECMWF too. To allow

---

[1] *https://github.com/mvdh7/CO2flux*
[2] *https://www. esrl.noaa.gov/gmd/ccgg/mbl/data.php*

for coherent calculations in agreement with the resolution of pCO_{2atm} from the SeaFlux toolbox, all available data (models described previously, Saildrone, BGC-Argo cruise, and mooring data) were gridded on a monthly 1°x1° resolution from January 2018 onwards.

2.3. Anthropogenic CO_2

Anthropogenic CO_2 (C_{ant}) emitted by human activities also penetrates the ocean and has a direct effect on ocean chemistry. Therefore, estimating C_{ant} concentrations in the ocean represents an important step toward a better evaluation of the global carbon budget and its rates of change. Since C_{ant} may not be directly measured in the ocean it has to be derived from *in situ* observations, using several assumptions. In more recent years, data-based methods have been developed in an attempt to improve the existing oceanic C_{ant} estimates, especially at a regional level (*e.g.* the TrOCA method, Touratier and Goyet, 2004; Touratier et al., 2007, the $C°_{IPSL}$ method, Lo Monaco et al., 2005, the φC_T^0 method, Vazquez-Rodriguez et al., 2009).

To study C_{ant} in the tropical Atlantic, we used BGC-Argo O_2 data combined with neural network methods and a C_{ant} estimation method. As nutrients and carbonate system variables were required by the back-calculation method, nutrients (nitrates, phosphates, silicates) were derived using the CANYONB neural networks (Bittig et al., 2018) at the O_2-equipped BGC-Argo float's sampling resolution in time and space. Carbonate variables, namely A_T and C_T, were derived using the CONTENT neural networks (Bittig et al, 2018). Then, to estimate C_{ant} from the total carbon pool, the back-calculation method φC_T^0 was used (Pérez et al., 2008). This method, originally developed for the Atlantic ocean requires temperature, salinity, and O_2 as well as nutrients, A_T, and C_T together with the location in time and space. It is a process-oriented biogeochemical approach to estimate C_{ant} in the Atlantic. The subsurface layer (100–200 m) is taken as a reference for characterizing water mass properties at the moment of their formation. The air-sea disequilibrium is parameterized at the subsurface layer (Matear et al., 2003) and conservative tracers parameterizations obtained from subsurface data are applied directly to calculate C_{ant} in the water column for waters above the 5°C isotherm and via an OMP analysis for waters with below the 5°C isotherm.

3. CO_2 and carbon fluxes in the tropical Atlantic

3.1. Variability within the tropical Atlantic

To better study the dynamic region that is the tropical Atlantic, it was necessary to subdivide it into coherent biogeochemical provinces (BGCPs) corresponding to unique regional environments that shape biodiversity and constrain ecosystem structures and functions rather than to look at it as one homogeneous area.

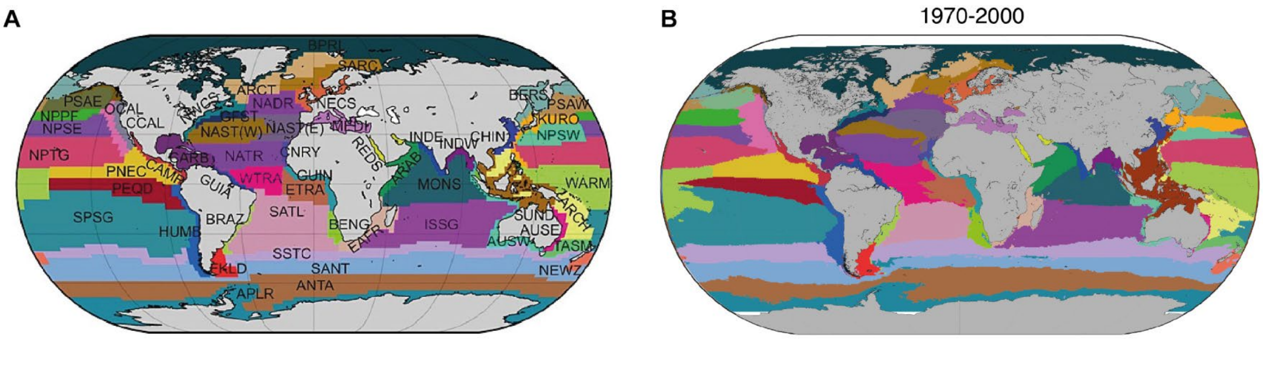

Figure 3. Distribution of the 56 BGCPs: (A) according to Longhurst (2007); and (B) for the average period 1970–2000. Distributions of each province were averaged across the three Earth System Models and three Environmental Niche Models. Each color represents a BGCP. Color coding refers to panel (A). Source: Reygondeau et al., 2020.

While the commonly accepted provinces were defined by Longhurst (2007; Figure 3A), they were revisited by Reygondeau et al. (2013, 2020, Figure 3B) to account for seasonal and interannual variability caused by phenomena such as the El Niño Southern Oscillation. These refined BGCPs have finer delimitations compared to Longhurst's coarse separations. However, data for these updated provinces were not available for our deliverable (contact with the first author), therefore, we used the 'classical' Longhurst provinces applied to the Tropical Atlantic.

Figure 3A presents the subdivision of the tropical Atlantic according to Longhurst's provinces and the *in situ* data used in this study in each area (Saildrone, BGC-Argo floats, moorings, cruises). The 9 provinces are the following: NATR (North Atlantic tropical gyral), CARB (Caribbean), CNRY (Canary current coast), GUIA (Guianas coast), WTRA (Western tropical Atlantic), GUIN (Guinea current coast), ETRA (Eastern tropical Atlantic), BRAZ (Brazilian current coast) and SATL (South Atlantic gyral). The BRAZ, GUIA, CNRY, and GUIN areas are coastal and might be subjected to riverine and anthropogenic influences.

The seasonal dynamics vary spatially. To provide a baseline when no *in situ* observations are available, $p\mathrm{CO}_{2sw}$ from the three models outputs used in this study were averaged per area at the monthly resolution. Figure 4 presents the seasonal variations over 2018-2021 for each province.

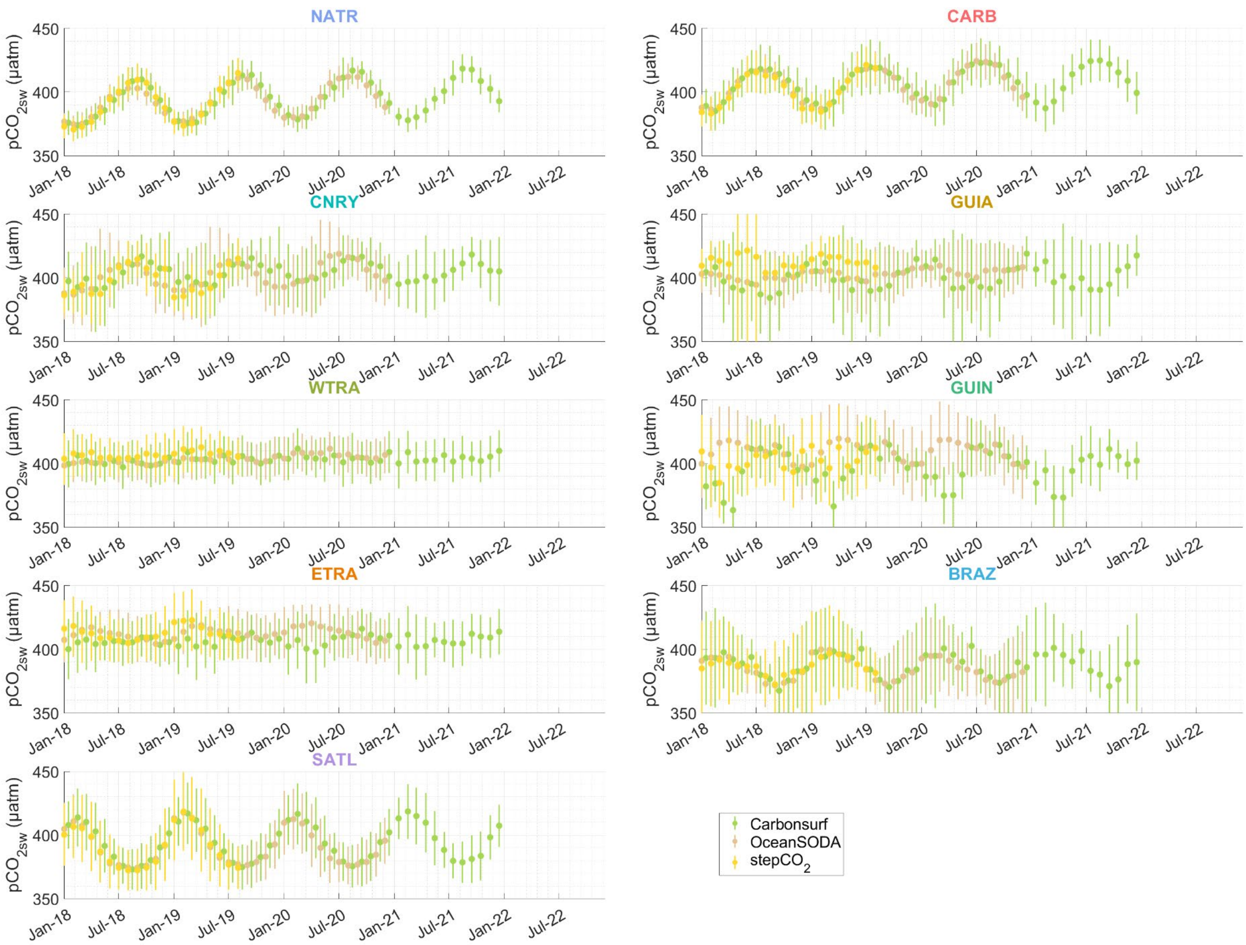

Figure 4. Surface pCO2sw averaged per area (± standard deviation) from Carbonsurf (Chau et al., 2022), OceanSODA (Gregor and Gruber, 2021), and stepCO2 (Zhong et al., 2022).

At the surface models globally agree on $p\mathrm{CO}_{2sw}$ except for the GUIN and GUIA BGCPs where larger differences occur. In these areas, the three models behave differently and disagree in the order of 50 to 70 µatm. This might be related to the coastal position of these areas with specific circulation features that receive the discharge of the two largest rivers of the world (Figure 1): the Amazon near the equator in the west (GUIA), and the Congo near 6°S in the east (GUIN). Furthermore, the large standard deviation might be related to the spatial variability within each area. Most areas exhibit a seasonal cycle with varying amplitudes from one BGCP to the other. The seasonality is small in the central WTRA and ETRA BGCPs (20 µatm of difference between summer and winter). In contrast, NATR, CARB, and SATL display well-defined large amplitude seasonal variations (50 µatm amplitude) with low variations inside each area. Therefore, the large discrepancies between models might be a sign of highly dynamic areas where the models did not sufficiently capture the biogeochemical processes because of a lack of training observations with respect to the region's dynamics.

3.2. Sea-air CO_2 fluxes

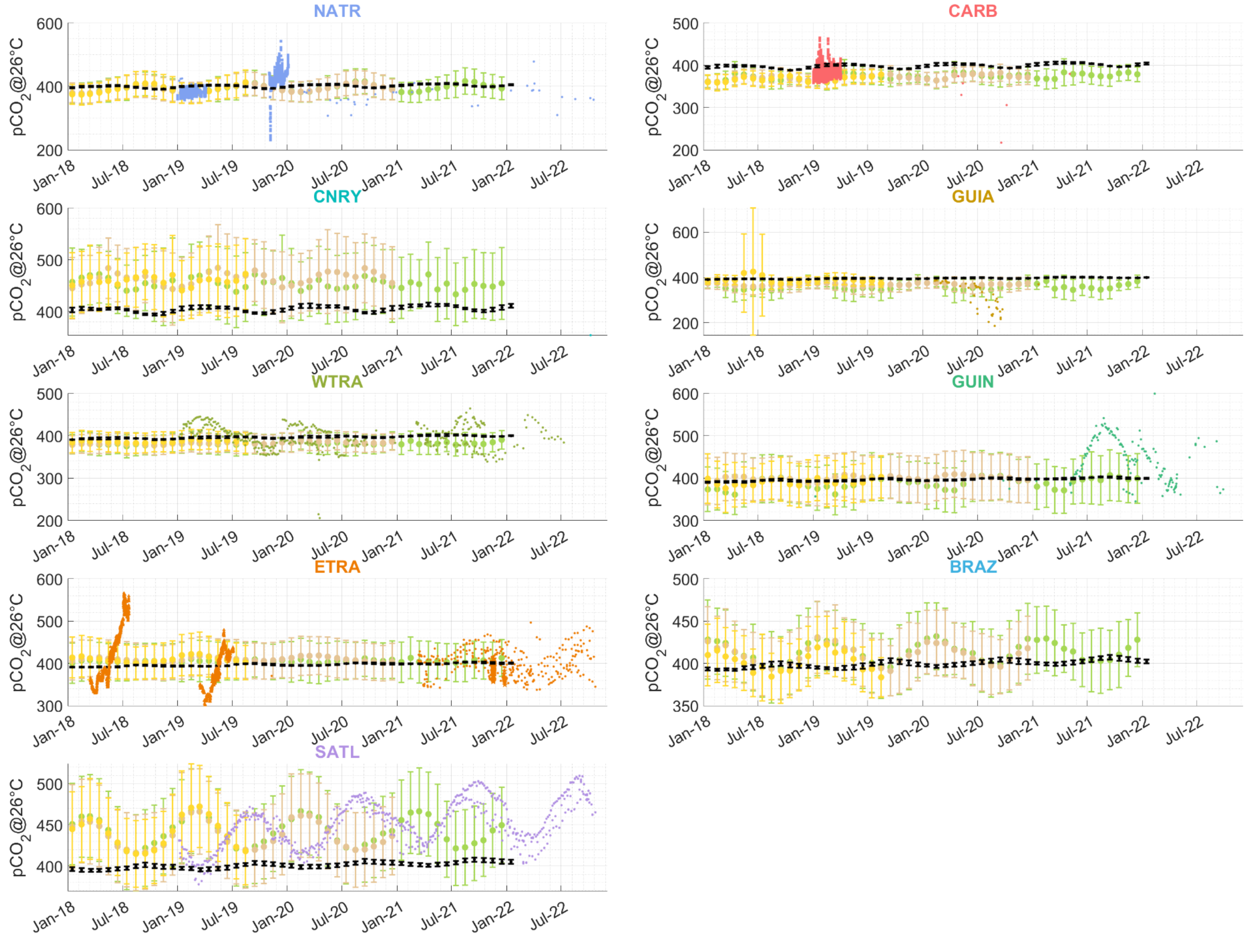

Figure 5. Surface pCO2sw normalized at 26°C according to Takahashi et al. (1993) averaged per area (and standard deviation) from Carbonsurf (Chau et al., 2022), OceanSODA (Gregor and Gruber, 2021), and stepCO2 (Zhong et al., 2022; same as figure 4) with in situ observations (Saildrone (stars), cruises (squares), Argo floats (dots), moorings (triangles)) coloured by area. Atmospheric pCO_2 from the Seaflux product (Fay et al., 2021) is averaged per area and is represented by the black markers. Note that the scale on the y-axis differs in each panel.

In most areas, pCO_{2sw}@26C from model predictions are in agreement with *in situ* measurements from cruises, BGC-Argo floats, Saildrone, and moorings except SATL, ETRA, and to some extent the GUIN BGCP. For ETRA, the model outputs do not reproduce the local variability captured by the mooring data from 2018 to 2020 with sharp increases beyond the model's ranges. The model data match the Saildrone data (stars at the end of 2021) which varies almost 40 µatm over a quasi-constant latitude, confirming the spatial variability, whereas pCO_{2sw}@26C from Argo floats display a wide range of values. For SATL, the seasonal cycle of Argo-derived pCO_{2sw}@26C presents a large offset (about 50 µatm) to model outputs with a reverse seasonal variation. This offset might highlight the poor performance of the neural networks used to derive pCO_{2sw} in this area. Indeed, for these three BGCPs, the pCO_{2sw} error is larger than in others and the errors are scattered across the vertical (over the first 2000 m, Supplementary Figure 1). This highlights the limitation of neural networks in specific areas where the training dataset was either too small or insufficient to adequately capture the biogeochemical variability in time and space. In addition, data products used in this study seem to smooth out local variability. This is to be expected as they were developed for the global ocean. Furthermore, it may be related to the fact that the mooring data are flagged 'E' in SOCAT, indicating they may be left out of the training of these data products. Atmospheric pCO_2 (black error bars, Figure 5) is relatively stable between and within BGCPs. In GUIA, WTRA, and NTRA, a similar decrease in 2020 is visible. This can directly be linked with the position of the Argo floats near the Amazon river outflow (Figure 1).

Air-sea CO_2 fluxes were computed (Figure 6, as described in section 2.2) for each BGCP and with each data acquisition platform available. For OceanSODA, Seaflux, and Carbsurf, FCO_2 was directly provided in the products. For Saildrone FCO_2 was calculated using the pCO_{2atm} and wind speed directly measured by the Saildrone (better matchup than with a model). For stepCO_2, cruise data, float data, and mooring data, FCO_2 was computed using pCO_{2atm} from Seaflux. Mirrored seasonality between NATR, CABR, and CNRY as opposed to SATL and BRAZ is consistent with the opposite hemispheres. Overall, most oceanic areas are CO_2 sinks (pCO_{2atm} higher than pCO_{2sw}) in winter and sources in summer. However, the WTRA and ETRA are almost continuous CO_2 sources. These areas closest to the Equator exhibit high SSTs throughout the year leading to CO_2 outgassing.

In GUIA and WTRA, a similar decrease from April to July 2020 is visible. This can directly be linked with the position of the Argo floats near the Amazon River outflow (Figure 1). Indeed, multiple studies (Cooley et al., 2007; Ibánhez et al., 2015; Körtzinger, 2003; Lefèvre et al., 2010, 2017; Ternon et al., 2000) have shown that the outflow of the Amazon River becomes a net sink of atmospheric CO_2 when the waters from the Amazonian plume mix with the surrounding ocean (lowering SSS) and alters the air-sea equilibrium of CO_2 in the region (Mu et al., 2021). The Amazon River plume waters are a strong net CO_2 sink, being responsible for 87% of the CO_2 uptake in the western Tropical Atlantic (Monteiro et al., 2022). In detail, the sink-to-source behavior in this area is determined by the balance between two sets of processes (Louchard et al., 2021): the riverine input of A_T favouring the sink and the outgassing caused by supplies of Dissolved Organic and Organic Carbon from the Amazon. This contrasted area has been subdivided recently by Monteiro et al. (2022) who identified three sub-regions: (1) a sub-region under the North Brazil Current, net source to the atmosphere, (2) a sub-region under the North Equatorial Current net CO_2 sink and (3) the Amazon River Plume directly influenced by the outflow.

The clear north-south gradient in the western tropical Atlantic near the Amazon (Lefévre et al., 2010; Takahashi et al., 2009) is visible in BGCPs NATR, WTRA, and GUIA with higher surface pCO_{2sw} in the south than further north because of the supply of CO_2 rich waters coming from below the equatorial upwelling (Lefèvre et al., 2014).

In the SATL, while models agree with cruises, float-based estimates differ largely from the Carbsurf estimate (up to 4 mmol $m^{-2}d^{-1}$), due to the bad prediction by neural networks in the area. In the ETRA, mooring-based FCO_2 estimates of -1 to 3 mmol $m^{-2}d^{-1}$ are consistent with previous estimates by Lefèvre et al., (2021) for 6°S 8°E. Furthermore, in ETRA the SD measurements were restricted to one season which might explain the small mismatch with the other estimates.

Estimates for each BGCP using a different combination of platforms were attempted (Supplementary Figure 2, Supplementary Text 1, Supplementary Table 1) but as the different datasets have different temporal resolutions, this comparison is marred by large errors and will not be presented more in this deliverable.

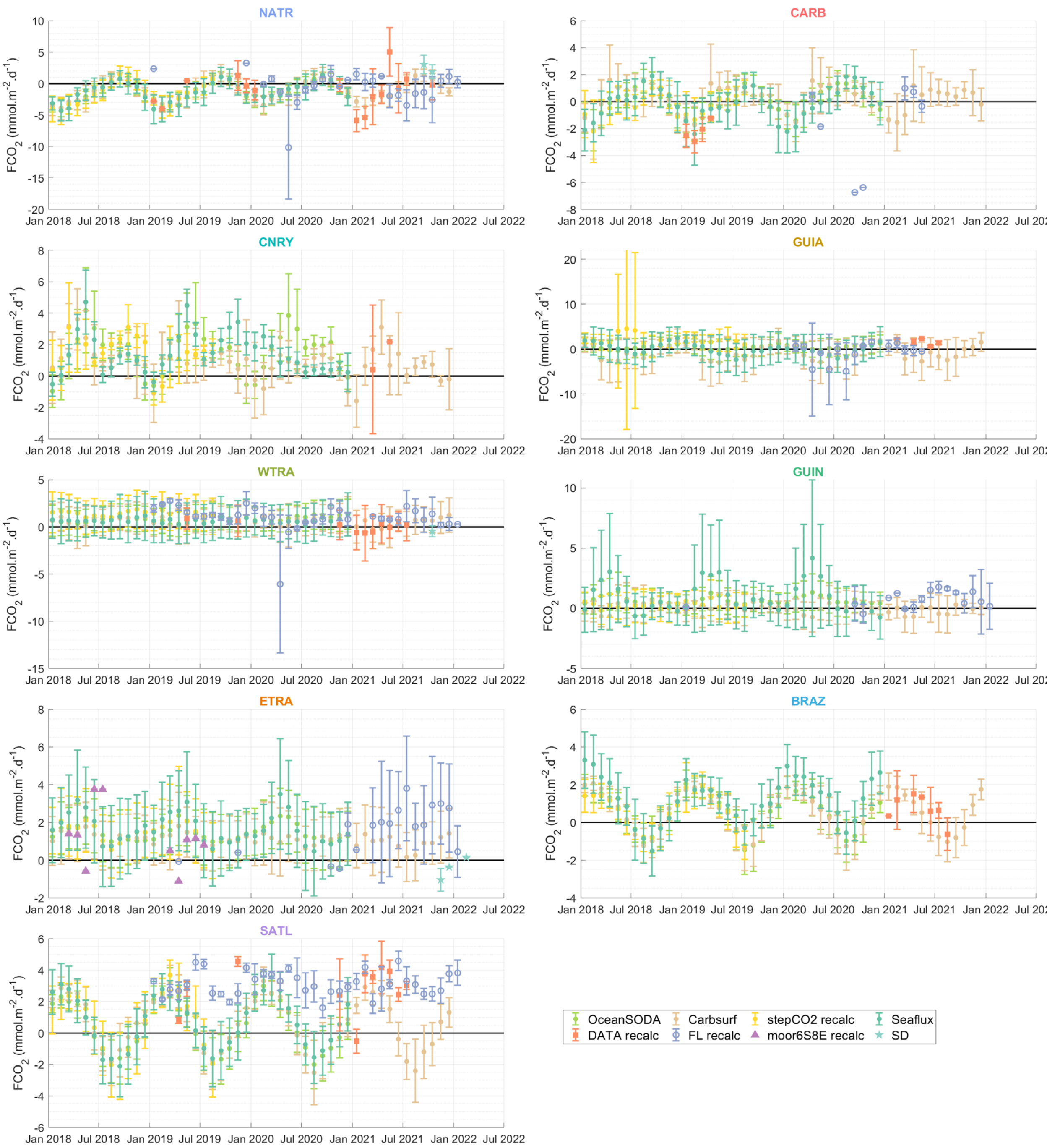

Figure 6. Time series of CO2 fluxes (FCO2) for each BGCP. FCO2 was recalculated for cruises (orange squares), Argo floats (grey circles), mooring (purple triangle), and for the stepCO2 model outputs (yellow dots). For the Saildrone (blue stars), Seaflux (turquoise dots), oceanSODA (green dots), and Carbsurf (brown dots) FCO_2 was directly provided and was not recalculated.

3.3. A look at anthropogenic Carbon

Monitoring and sustained observations of surface oceanic CO_2 are critical for understanding the fate of CO_2 as it penetrates the ocean. Looking at C_{ant} allows the understanding of where this CO_2 will accumulate. The concentration of C_{ant} is not homogeneous over the water column as higher values are found near the surface where it accumulates with atmospheric exchanges. The concentration then decreases with depth. Over time and in correlation with the atmospheric increase in CO_2, C_{ant} also increases throughout the water column. In the same BGCPs as previously, C_{ant} was derived from the φC_T^0 method (Vazquez-Rodriguez et al., 2009) applied on BGC-Argo floats (see details in section 2.3). To study C_{ant} storage over the vertical, profiles were regularised and integrated over the first 1000 dbar (Figure 7, shallowest limiting depth reached by all floats).

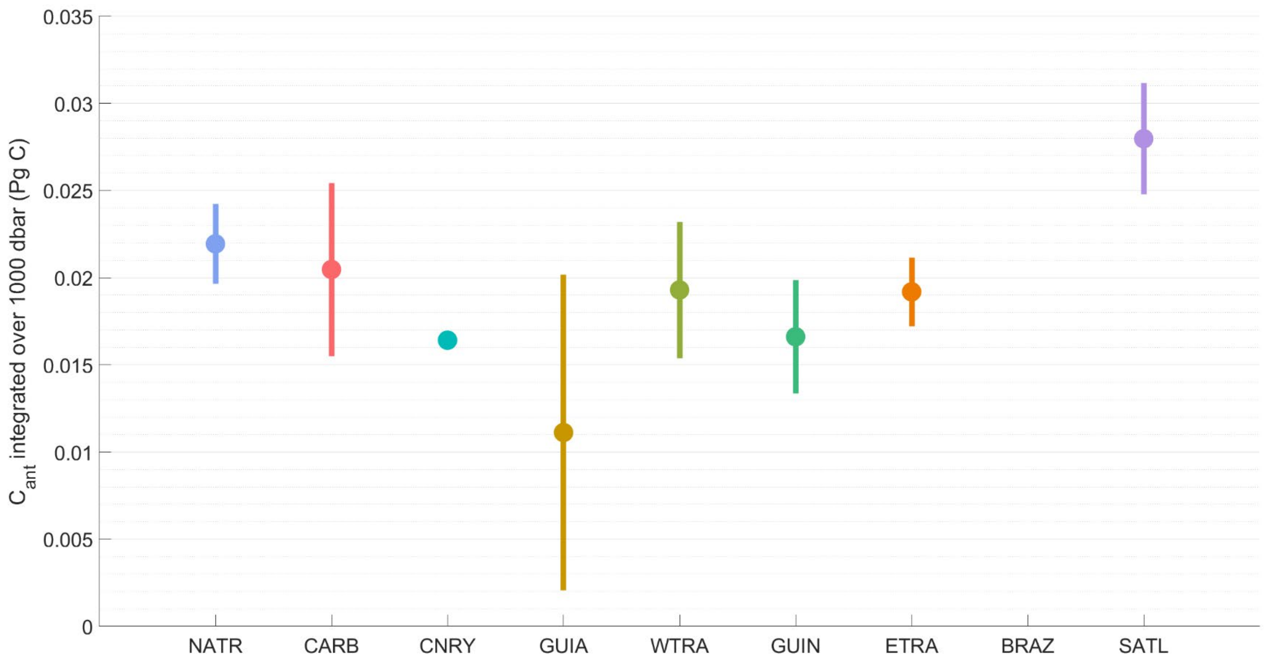

Figure 7. Integrated Cant (mean ± standard deviation) over the first 1000 dbar and the period 2018-2021 multiplied by the surface of each area derived using the φC_T^0 method, Vazquez-Rodriguez et al., (2009) on Argo floats in each BGCP.

There is substantial anthropogenic carbon uptake in the tropical Atlantic. While a portion of this tropical uptake is transported southwards, most of it is either stored in the tropics or transported northwards along the surface before being stored in the subtropical North Atlantic (Mikaloff Fletcher et al., 2006). The largest C_{ant} integrated over the period 2018-2021 occurs in the SATL (0.028 ± 0.003 Pg C) and we find the largest variability in GUIA (0.011 ± 0.009 Pg C) subjected to the Amazonian output. Over the 2000s, Woosley et al. (2016) estimated a C_{ant} inventory of 1.97 Pg C.decade^{-1} while Lee et al. (2003) produced an estimate of 10 ± 3.1 Pg C over the 20°S-20°N band more than ten times our estimate. Our C_{ant} estimates applying the φC_T^0 method on BGC-Argo floats are therefore not directly comparable to previous estimates as they are restricted to the first 1000 dbar of the water column.

3.4. Insights into optimizing observing systems

Numerous sensor platforms exist for directly measuring or deriving oceanic pCO_2, as used in this report. A qualitative description of some cost-benefit information for these platforms is given in Table 1.

Table 1. Cost, measurement frequency, and uncertainty associated with different oceanic CO_2 observing platforms

Observing platform	**Cost**	**Measurement frequency**	**pCO_2 associated uncertainty**	**Type of measurements**
CO_2-equipped mooring	~50 k€ for the CARIOCA sensor	Hourly	<10 µatm	Surface
Saildrone	~2 k€ per day	Every 30 minutes	<4 µatm	Surface
Yearly cruise (PIRATA)	~650-900 €[3]	5 profiles (10 depths) and 10-30 surface measurements	8-16 µatm[4]	Water column
SOOP line	~80 k€ (ferrybox) + maintenance costs	Every 3 minutes	2 µatm	Surface
BGC-Argo float	~50 k€ for a float equipped with O_2 and pH	Every 1-10 days [5]	6.5-25 µatm[6]	Water column

Saildrones and Ships of Opportunity (SOOP lines) are among the best quality measurements for investigating oceanic pCO_2 with the lowest uncertainties as they have onboard reference gases. However, Saildrones represent a large financial investment, while SOOP lines, as their name suggests, collect data with no direct choice of sampling season and/or trajectory. The deployment of CO_2 sensors on moorings in the tropical Atlantic (in the PIRATA network) has allowed the acquisition of time series and the study of seasonal and interannual variations of surface pCO_{2sw} (Bourlès et al., 2019; Lefèvre et al., 2013,2021). However, these sensors are subject to harsh weather conditions and piracy and require annual maintenance. This maintenance is often coupled with the annual PIRATA cruises where A_T and C_T are sampled for analysis. From these *in* situ bottle sampling of the carbonate system, pCO_{2sw} can be derived (with uncertainties ranging from 8 to 16 µatm, Table 1). There is no direct pCO_{2sw} measurement along the research vessel track, but the addition of a ferry box (such as on SOOP lines) could be useful to easily extend the measurements. These cruises also allow the periodic sampling of the entire water column for carbonate system variables, enabling the study of the sequestration of CO_2 after its absorption at the surface. These repeated cruises can also be very useful for deploying BGC-Argo floats and having *in situ* reference data to adjust the floats' sensors. In particular, O_2- and pH-equipped BGC-Argo floats combined with A_T from neural network methods (e.g. CONTENT, Bittig et al., 2018 as in this deliverable) can allow us to obtain pCO_2 at the surface and along the water column.

However, the development of an OSSE (Observing System Simulation Experiment) would be required to comprehensively determine the optimal combination of observing platforms for the study of oceanic CO_2. Thus, the qualitative elements of the different observing platforms mentioned above might pave the way for such a design, as done by Denvil-Sommer et al. (2021), who assessed the impact of the addition of Argo floats (with varying spatial coverage) and mooring arrays on the reconstruction of surface oceanic pCO_2 in the

[3] This represents only the cost for the A_T and C_T analysis.
[4] For sample analysis accuracies from 1,5 to 3 µmol/kg for A_T and C_T.
[5] Throughout the life of the float, this cycling frequency can be changed. On average, the new BGC-Argo floats have enough battery life for ~300 profiles.
[6] For a neural-network A_T error of 6.2 µmol/kg (CONTENT, Bittig et al., 2018) and a float-based pH error from 0.005 to 0.02 pH units (depending on sensor failures and quality of delayed-mode adjustments).

Atlantic Ocean. Their focus was on the short-term interannual variability of pCO_2, which is similar to the time scale of the present study. Coastal regions such as our GUIN BGCP have pronounced biases in all OSSEs. This could be substantially improved by the addition of moorings, gliders, as well as Saildrones and sail buoys along the continental shelf (Denvil-Sommer et al., 2021).

We recommend that the next step is a comprehensive OSSE, building on Denvil-Sommer et al. (2021) in terms of sampling locations and insights into where large pCO_2 uncertainties remain in calculating air-sea CO_2 fluxes. Therefore, an OSSE including *in situ* errors would explicitly help to define where to use the different observation platforms (Saildrones, BGC Argo floats, moorings) to best improve our coverage of the oceanic pCO_2 system.

Conclusion

The tropical Atlantic is a very contrasted area that has been determined as the second largest source of CO_2 to the atmosphere (Landschützer et al., 2014). It is affected by multiple physical and biogeochemical processes, varying on many time scales and impacting surrounding areas (Foltz et al., 2019). Furthermore, this area is known to exhibit significant interannual variability of air-sea CO_2 fluxes closely linked to climate variability (Lefèvre et al., 2013; Ibánhez et al., 2017). The tropical Atlantic observing system has progressed substantially over the past two decades. Still, many challenges and uncertainties remain requiring further studies into the area's role in terms of carbon fluxes (Foltz et al., 2019). Monitoring and sustained observations of surface oceanic CO_2 are critical for understanding the fate of CO_2 as it penetrates the ocean and afterwards.

Using a combination of multi-platform observations, models, and neural network techniques, this deliverable allowed us to assess our ability to derive air-sea CO_2 fluxes in the tropical Atlantic over the period 2018-2021. This deliverable builds on the work done in EuroSea D7.1 and D7.2 which describe the observing platforms deployed in the tropical Atlantic as part of the EuroSea project (notably Saildrone and BGC-Argo floats) and the correction of their data to ensure good quality observations. However, it should be mentioned that further work is necessary to ensure the availability of model outputs and data products (*i.e.* unavailable updated BGCPs which would have been helpful to precise the work done in this deliverable).

Overall, the tropical Atlantic is a source of CO_2 to the atmosphere with high variability (seasonal and interannual) in the GUIA and GUIN BGCPs, consistent with the literature. The use of data products, while very useful in filling gaps, remains limited as these data products often do not adequately represent the large spatial and/or seasonal variability intrinsic to the area. There is still a great need for sustained observations, either by using vessels of opportunity that provide regular high-quality monitoring of specific areas (such as the France-Brazil SOOP line) or by developing specific pilot observation experiments such as the one implemented in EuroSea. Indeed, a Saildrone, BGC-Argo floats equipped with pH sensors have been deployed and collocated matchups between these platforms, moorings, and cruises have been carried out. It is also important to emphasize that there is only one CO_2 mooring left in the area (part of the PIRATA network). It is difficult to maintain long-term datasets due to harsh conditions, sensor problems, and piracy. In addition, there is a need to further improve the ability of platforms to accurately measure the variables needed to estimate CO_2 fluxes (e.g. acoustic wind measurements on Argo floats). It is also necessary to continue to improve sensor technology to provide reliable measurements over the long term. This, combined with a good observation strategy and QC algorithm procedures, will allow us to improve CO_2 products. Saildrones provide high-quality data and have the advantage of onboard collocated measurements of wind speed and atmospheric CO_2 needed to derive air-sea CO_2 fluxes. However, this high-frequency dataset is not the most cost-effective and we should not rely solely on these types of platforms to study entire ocean basins.

Saildrones can be used, as it has been done in EuroSea (matchups with Argo floats and moorings), as a tool to link platforms. Neural networks allow gaps to be filled and provide CO_2 estimates by enhancing limited T/S/O_2 datasets with given uncertainties. When used in combination with pH sensors mounted on BGC-Argo floats, they help derive $p$$CO_2$ with reduced uncertainties.

We suggest that an effective and economical way to monitor the area and ensure comparisons between platforms, as well as providing the accurate dataset needed to improve neural network training and prediction, could be pilot studies with permanent 'rendezvous' between different monitoring platforms. In addition, an OSSE including *in situ* errors would explicitly help to define where to use the different observation platforms (Saildrones, BGC Argo floats, moorings) to best improve our coverage of the oceanic $p$$CO_2$ system.

Data availability statement

Fully processed and finalised surface $p$$CO_2$ data have been submitted in 2023 to the Surface Ocean CO_2 Atlas (SOCAT) for community-based quality control and final ingestion into global carbon synthesis products and assessments. Argo data are available at http://doi.org/10.17882/42182#96550 or at ftp://ftp.ifremer.fr/ifremer/argo/dac/coriolis. These data were collected and made freely available by the International Argo Program and the national programs that contribute to it[7]. The Argo Program is part of the Global Ocean Observing System. Data from the french PIRATA cruises are available on the SEANOE website[8]. Mooring data is available in SOCAT.

Acknowledgements

We acknowledge the “Flotte Oceanographique Francaise”, FOF, and the crew of the R/V “La Thalassa” (IFREMER) for their help in the PIRATA-FR31 and -32 sampling. The many researchers responsible for the collection of data and quality control are thanked for their contribution, as well as the teams working on SOCAT. For pH seawater sampling and analyses, particular thanks to Pierre Rousselot, Thierry Cariou and Sandrine Hillion (IRD, UAR191, Instrumentation, Moyens Analytiques, Observatoires en Geophysique et Oceanographie (IMAGO), Technopole de Brest-Iroise, Plouzane, France). For Argo deployments in the area during PIRATA cruises, we thank Bernard Bourles. We also thank Nathalie Lefevre for her valued contribution to the FR-SOOP-France-Brazil line (LOCEAN/IPSL). Thanks are also given to Nicolas Metzl for fruitful discussions on CO_2 comparisons.

[7] https://argo.ucsd.edu, https://www.ocean-ops.org
[8] https://www.seanoe.org

References

Bakker, D. C. E., Pfeil, B., Landa, C. S., Metzl, N., O'Brien, K. M., Olsen, A., et al. (2016). A multi-decade record of high-quality CO2 data in version 3 of the Surface Ocean CO2 Atlas (SOCAT). Earth System Science Data, 8(2), 383–413. https://doi.org/10.5194/essd-8-383-2016

Bittig, H. C., Steinhoff, T., Claustre, H., Fiedler, B., Williams, N. L., Sauzède, R., et al. (2018). An Alternative to Static Climatologies: Robust Estimation of Open Ocean CO2 Variables and Nutrient Concentrations From T, S, and O2 Data Using Bayesian Neural Networks. Frontiers in Marine Science, 5. https://doi.org/10.3389/fmars.2018.00328

Boers, N., 2021. Observation-based early-warning signals for a collapse of the Atlantic Meridional Overturning Circulation. Nature Climate Change, 11, 21.

Bourlès, B., Brandt, P., Lefèvre, N. and Hahn, J., 2018. AtlantOS EU H2020 633211 Deliverable 3.9 "PIRATA data system upgrade report: Technical report mostly related to biogeochemical sensors (O2 and CO2 sensors) data, their real-time transmission and O2 and CO2 data control quality and their integration to existing systems, in relation with the WP7", https://doi.org/10.3289/AtlantOS_D3.9.

Bourlès, B., Araujo, M., McPhaden, M. J., Brandt, P., Foltz, G. R., Lumpkin, R., et al. (2019). PIRATA: A Sustained Observing System for Tropical Atlantic Climate Research and Forecasting. Earth and Space Science, 6(4), 577–616. https://doi.org/10.1029/2018EA000428

Chau, T. T. T., Gehlen, M., & Chevallier, F. (2022). A seamless ensemble-based reconstruction of surface ocean CO2 and air–sea CO2 fluxes over the global coastal and open oceans. Biogeosciences, 19(4), 1087–1109. https://doi.org/10.5194/bg-19-1087-2022

Cooley, S. R., Coles, V. J., Subramaniam, A., & Yager, P. L. (2007). Seasonal variations in the Amazon plume-related atmospheric carbon sink. Global Biogeochemical Cycles, 21(3), GB3014. https://doi.org/10.1029/2006GB002831

Denvil-Sommer, A., Gehlen, M., and Vrac, M.: Observation system simulation experiments in the Atlantic Ocean for enhanced surface ocean pCO_2 reconstructions, Ocean Sci., 17, 1011–1030, https://doi.org/10.5194/os-17-1011-2021, 2021

Dickson, A. G., C. L. Sabine, and J. R. Christian (Eds.), 2007. Guide to Best Practices for Ocean CO2 Measurements. PICES Special Publication 3, 191 pp.

Dickson, A. G., & Millero, F. J. (1987). A comparison of the equilibrium constants for the dissociation of carbonic acid in seawater media. Deep Sea Research, 34(10), 1733–1743.

Dlugokencky, E. J., Thoning, K. W., Lang, P. M., and Tans, P. P.: NOAA Greenhouse Gas Reference from Atmospheric Carbon Dioxide Dry Air Mole Fractions from the NOAA ESRL Carbon Cycle CooperativeGlobal Air Sampling Network, 2019 (data available at: https://www.esrl.noaa.gov/gmd/ccgg/mbl/data.php).

Fay, A. R., Gregor, L., Landschützer, P., McKinley, G. A., Gruber, N., Gehlen, M., et al. (2021). SeaFlux: harmonization of air–sea CO2 fluxes from surface CO2 data products using a standardized approach. Earth System Science Data, 13(10), 4693–4710. https://doi.org/10.5194/essd-13-4693-2021

Fiedler, B., Cancouet, R., Claustre, H., Coppola, L., Cotrim da Cunha, L., Fourrier, M., Hernandez, F., Paulsen, M. and Wimart-Rousseau, C. (2022). Report on demo mission and dissemination pathways of obtained data based on different observational platforms. EuroSea Deliverable, D7.1. EuroSea, 31 pp. https://doi.org/10.3289/eurosea_d7.1.

Foltz, G.R., et al., 2019. The Tropical Atlantic Observing System. Frontiers in Marine Science, 6: 1-36.

Friedlingstein, P., O'Sullivan, M., Jones, M. W., Andrew, R. M., Gregor, L., Hauck, J., et al. (2022). Global Carbon Budget 2022. Earth System Science Data, 14(11), 4811–4900. https://doi.org/10.5194/essd-14-4811-2022

Goni, G., Roemmich, D., Molinari, R., Meyers, G., Sun, C., Boyer, T., Baringer, M., Gouretski, V., DiNezio, P., Reseghetti, F., Vissa, G., Swart, S., Keeley, R., Garzoli, S., Rossby, T., Maes, C. and Reverdin, G., 2010. The Ship of Opportunity program, Proceedings of OceanObs'09: Sustained Ocean Observations and Information for Society, (Vol. 2). Venice, Italy: ESA Publication.

Good, S. A., Martin, M. J., and Rayner, N. A.: EN4: Quality controlled ocean temperature and salinity profiles and monthly objective analyses with uncertainty estimates, J. Geophys. Res.-Oceans, 118, 6704–6716, https://doi.org/10.1002/2013JC009067, 2013.

Gregor, L.: luke-gregor/OceanSODA-ETHZ: code, Zenodo, https://doi.org/10.5281/zenodo.4455354, 2021.

Gregor, L. and Gruber, N.: OceanSODA-ETHZ: a global gridded data set of the surface ocean carbonate system for seasonal to decadal studies of ocean acidification, Earth Syst. Sci. Data, 13, 777–808, https://doi.org/10.5194/essd-13-777-2021, 2021.

Hersbach, H., Bell, B., Berrisford, P., Hirahara, S., Horányi, A., Muñoz-Sabater, J., Nicolas, J., Peubey, C., Radu, R., Schepers, D., Simmons, A., Soci, C., Abdalla, S., Abellan, X., Balsamo, G., Bechtold, P., Biavati, G., Bidlot, J., Bonavita, M., De Chiara, G., Dahlgren, P., Dee, D., Diamantakis, M., Dragani, R., Flemming, J., Forbes, R., Fuentes, M., Geer, A., Haimberger, L., Healy, S., Hogan, R.J., Hólm, E., Janisková, M., Keeley, S., Laloyaux, P., Lopez, P., Lupu, C., Radnoti, G., de Rosnay, P., Rozum, I., Vamborg, F., Villaume, S., and Thépaut, J.: The ERA5 global reanalysis, Q. J. Roy. Meteor. Soc. 146, 1999–2049, https://doi.org/10.1002/qj.3803, 2020).

Huang, B., Thorne, P. W., Banzon, V. F., Boyer, T., Chepurin, G., Lawrimore, J. H., Menne, M. J., Smith, T. M., Vose, R. S., and Zhang, H.-M.: Extended reconstructed sea surface temperature, version 5 (ERSSTv5): upgrades, validations, and intercomparisons, J. Climate, 30, 8179–8205, 2017.

Ibánhez, J. S. P., Flores, M., and Lefèvre, N. (2017). Collapse of the tropical and subtropical North Atlantic CO2 sink in boreal spring of 2010. Sci. Rep. 7, 1–9. doi: 10.1038/srep41694

Ibánhez, J. S. P., Diverrès, D., Araujo, M., & Lefèvre, N. (2015). Seasonal and interannual variability of sea-air CO2 fluxes in the tropical Atlantic affected by the Amazon River plume. Global Biogeochemical Cycles, 29(10), 1640–1655.

Johnson, K. S., Plant, J. N., Coletti, L. J., Jannasch, H. W., Sakamoto, C. M., Riser, S. C., et al., 2017. Biogeochemical sensor performance in the SOCCOM profiling float array. Journal of Geophysical Research: Oceans, 122(8), 6416–6436.

Körtzinger, A. (2003). A significant CO2 sink in the tropical Atlantic Ocean associated with the Amazon River plume. Geophysical Research Letters, 30(24). https://doi.org/10.1029/2003GL018841

Landschützer, P., Gruber, N., Bakker, D. C. E., and Schuster, U., 2014. Recent variability of the global ocean carbon sink. Glob. Biogeochem. Cycles 28: 927–949.

Lauvset, S. K., Lange, N., Tanhua, T., Bittig, H. C., Olsen, A., Kozyr, A., et al. (2022). GLODAPv2.2022: the latest version of the global interior ocean biogeochemical data product. Earth System Science Data, 14(12), 5543–5572. https://doi.org/10.5194/essd-14-5543-2022.

Lee, K., et al., An updated anthropogenic CO_2 inventory in the Atlantic Ocean, Global Biogeochem. Cycles, 17(4), 1116, doi:10.1029/2003GB002067, 2003

Lefévre, N., Diverrés, D., & Gallois, F. (2010). Origin of CO2 undersaturation in the western tropical Atlantic. Tellus B: Chemical and Physical Meteorology, 62(5), 595–607. https://doi.org/10.1111/j.1600-0889.2010.00475.x

Lefèvre, N., Caniaux, G., Janicot, S., and Gueye, A. K. (2013). Increased CO2 outgassing in February-May 2010 in the tropical Atlantic following the 2009 Pacific El Niño. J. Geophys. Res. 118, 1645–1657. doi: 10.1002/jgrc.20107.

Lefèvre, N., Urbano, D. F., Gallois, F., & Diverres, D. (2014). Impact of physical processes on the seasonal distribution of the fugacity of CO2 in the western tropical Atlantic. Journal of Geophysical Research: Oceans, 1–18. https://doi.org/10.1002/2013JC009248.

Lefèvre, N., Flores Montes, M., Gaspar, F. L., Rocha, C., Jiang, S., De Araújo, M. C., & Ibánhez, J. S. P. (2017). Net heterotrophy in the Amazon continental shelf changes rapidly to a sink of CO2 in the outer Amazon plume. Frontiers in Marine Science, 4, 278. https://doi. org/10.3389/fmars.2017.00278

Lefèvre, N., Mejia, C., Khvorostyanov, D., Beaumont, L., & Koffi, U. (2021). Ocean Circulation Drives the Variability of the Carbon System in the Eastern Tropical Atlantic. Oceans, 2(1), 126–148. https://doi.org/10.3390/oceans2010008.

Lewis, E., & Wallace, D. W. R. (1998). Program developed for CO2 system calculations.

Lo Monaco, C., Metzl, N., Poisson, A., Brunet, C., and Schauer, B.: Anthropogenic CO2 in the Southern Ocean: Distribution and inventory at the Indian-Atlantic boundary (World Ocean Circulation Experiment line I6), J. Geophys. Res., 110, C06010, doi:10.1029/2004JC002643, 2005.

Longhurst, A. (2007). Ecological Geography of the Sea. Cambridge, MA: Academic Press.

Louchard, D., Gruber, N., & Münnich, M. (2021). The Impact of the Amazon on the Biological Pump and the Air-Sea CO 2 Balance of the Western Tropical Atlantic. Global Biogeochemical Cycles, 35(6). https://doi.org/10.1029/2020GB006818

Marshall, G. J.: Trends in the Southern Annular Mode from observations and reanalyses, J. Climate, 16, 4134–4143, https://doi.org/10.1175/1520-0442(2003)016%3C4134:TITSAM%3E2.0.CO;2, 2003.

Maurer, T. L., Plant, J. N., & Johnson, K. S., 2021. Delayed-mode quality control of oxygen, nitrate and pH data on SOCCOM biogeochemical profiling floats. Front. Mar. Sci., 8:683207.

Matear, R. J., Wong, C. S., and Xie, L.: Can CFCs be used to determine anthropogenic CO2, Global Biogeochem. Cy., 17(1), 1013, doi:10.1029/2001GB001415, 2003.

Mehrbach, C., Culberson, C. H., Hawley, J. E., & Pytkowicx, R. M. (1973). Measurement of the apparent dissociation constants of carbonic acid in seawater at atmospheric pressure. Limnology and Oceanography, 18(6), 897–907. https://doi.org/10.4319/lo.1973.18.6.0897

Mikaloff Fletcher, S. E., et al. (2006), Inverse estimates of anthropogenic CO2 uptake, transport, and storage by the ocean, Global Biogeochem. Cycles, 20, GB2002, doi:10.1029/2005GB002530.

Monteiro, T., Batista, M., Henley, S., Machado, E. da C., Araujo, M., & Kerr, R. (2022). Contrasting Sea-Air CO2 Exchanges in the Western Tropical Atlantic Ocean. Global Biogeochemical Cycles, 36(8). https://doi.org/10.1029/2022GB007385

Mu, L., Gomes, H. do R., Burns, S. M., Goes, J. I., Coles, V. J., Rezende, C. E., et al. (2021). Temporal Variability of Air-Sea CO 2 flux in the Western Tropical North Atlantic Influenced by the Amazon River Plume. Global Biogeochemical Cycles, 35(6). https://doi.org/10.1029/2020GB006798

Olsen, A., Key, R. M., van Heuven, S., Lauvset, S. K., Velo, A., Lin, X., et al. (2016). The Global Ocean Data Analysis Project version 2 (GLODAPv2) – an internally consistent data product for the world ocean. Earth System Science Data, 8(2), 297–323. https://doi.org/10.5194/essd-8-297-2016.

Orr, J. C., Epitalon, J.-M., Dickson, A. G., & Gattuso, J.-P. (2018). Routine uncertainty propagation for the marine carbon dioxide system. Marine Chemistry, 207, 84-107. https://doi.org/10.1016/j.marchem.2018.10.006

Padin, X. A., Vázquez-Rodríguez, M., Castaño, M., Velo, A., Alonso-Pérez, F., Gago, J., Gilcoto, M., Álvarez, M., Pardo, P. C., de la Paz, M., Ríos, A. F., and Pérez, F. F.: Air-Sea CO_2 fluxes in the Atlantic as measured during boreal spring and autumn, Biogeosciences, 7, 1587–1606, https://doi.org/10.5194/bg-7-1587-2010, 2010

Park, G.-H., and Wanninkhof, R. (2012). A large increase of the CO2 sink in the western tropical North Atlantic from 2002 to 2009. J. Geophys. Res. 117:C080029. doi: 10.1029/2011JC007803

Pérez, F. F., and Fraga, F. (1987). A precise and rapid analytical procedure for alkalinity determination. Mar. Chem. 21, 169–182. doi: 10.1016/0304-4203(87)90037-5

Pérez, F. F., Vázquez-Rodríguez, M., Louarn, E., Padín, X. A., Mercier, H., and Ríos, A. F.: Temporal variability of the anthropogenic CO2 storage in the Irminger Sea, Biogeosciences, 5, 1669–1679, 2008,

Reygondeau, G., Longhurst, A., Martinez, E., Beaugrand, G., Antoine, D., & Maury, O. (2013). Dynamic biogeochemical provinces in the global ocean. Global Biogeochemical Cycles, 27(4), 1046–1058. https://doi.org/10.1002/gbc.20089

Reygondeau, G., Cheung, W. W. L., Wabnitz, C. C. C., Lam, V. W. Y., Frölicher, T., & Maury, O. (2020). Climate Change-Induced Emergence of Novel Biogeochemical Provinces. Frontiers in Marine Science, 7, 657. https://doi.org/10.3389/fmars.2020.00657

Reynolds, R. W., Rayner, N. A., Smith, T. M., Stokes, D. C., and Wang, W.: An improved in situ and satellite SST analysis for climate, J. Climate, 15, 1609–1625, https://doi.org/10.1175/15200442(2002)015<1609:AIISAS>2.0.CO;2, 2002.

Speich, S., Lee, T., Muller-Karger, F., Lorenzoni, L., Pascual, A., Jin, D., et al. (2019). Editorial: Oceanobs'19: An Ocean of Opportunity. Frontiers in Marine Science, 6. https://doi.org/10.3389/fmars.2019.00570

Sutton, A. J. and Sabine, C. L. and Maenner-Jones, S. and Lawrence-Slavas, N. and Meinig, C. and Feely, R. A. and Mathis, J. T. and Musielewicz, S. and Bott, R. and McLain, P. D. and Fought, H. J. and Kozyr, A., 2014. A high-frequency atmospheric and seawater pCO2 data set from 14 open-ocean sites using a moored autonomous system. Earth System Science Data, 6 (2): 353-366.

Takahashi T., Olafsson J., Goddard J.G. et al., "Seasonal variation of CO2 and nutrients in the high latitude surface oceans. A comparative study", Global Biogeochemical Cycles, vol. 7, pp. 843–878, 1993.

Takahashi, T., Sutherland, S. C., Wanninkhof, R., Sweeney, C., Feely, R. A., Chipman, D. W., et al. (2009). Climatological mean and decadal change in surface ocean pCO2, and net sea-air CO2 flux over the global oceans. Deep Sea Research Part II: Topical Studies in Oceanography, 56(8–10), 554–577. https://doi.org/10.1016/j.dsr2.2008.12.009

Takahashi, T., S.C. Sutherland and A. Kozyr (2019). Global Ocean Surface Water Partial Pressure of CO2 Database (LDEO Database Version 2019): Measurements Performed During 1957–2019 (NCEI Accession 0160492). NOAA National Centers for Environmental Information. Dataset.

Ternon, J. F., Oudot, C., Dessier, A., & Diverres, D. (2000). A seasonal tropical sink for atmospheric CO2 in the Atlantic ocean: The role of the Amazon River discharge. Marine Chemistry, 68(3), 183–201. https://doi.org/10.1016/S0304-4203(99)00077-8

Touratier, F. and Goyet, C.: Applying the new TrOCA approach to estimate the distribution of anthropogenic CO2 in the Atlantic Ocean, J. Mar. Sys., 46, 181–197, 2004.

Touratier, F., L. Azouzi & C. Goyet (2007). CFC-11, Δ14C and 3H tracers as a means to assess anthropogenic CO2 concentrations in the ocean, Tellus B: Chemical and Physical Meteorology, 59:2, 318-325

Uppström, L. R. (1974). The boron/chlorinity ratio of deep-sea water from the Pacific Ocean. Deep Sea Research, 21, 161–162.

van Heuven, S., D. Pierrot, J.W.B. Rae, E. Lewis, and D.W.R. Wallace, 2011. MATLAB Program Developed for CO2 System Calculations. ORNL/CDIAC-105b. Carbon Dioxide Information Analysis Center, Oak Ridge National Laboratory, U.S. Department of Energy, Oak Ridge, Tennessee.

Vazquez-Rodrıguez, M., Touratier, F., Monaco, C. L., Waugh, D. W., Padin, X. A., Bellerby, R. G. J., et al. (2009). Anthropogenic carbon distributions in the Atlantic Ocean: data-based estimates from the Arctic to the Antarctic. Biogeosciences, 6(439–451), 13.

von Schuckmann, K., P.-Y. Le Traon, N. Smith, A. Pascual, S. Djavidnia, P. Brasseur, M. Grégoire (Eds.) (2022). Copernicus Ocean State Report, Issue 6, Journal of Operational Oceanography, 15:sup1, s1–s220; DOI: 10.1080/ 1755876X.2022.2095169

Wanninkhof, R.: Relationship between wind speed and gas exchange over the ocean, J. Geophys. Res., 97, 7373, https://doi.org/10.1029/92JC00188, 1992.

Wanninkhof, R., 2014. Relationship between wind speed and gas exchange over the ocean revisited: Gas exchange and wind speed over the ocean. Limnology and Oceanography: Methods, 12 (69): 351-362.

Watson, A., Lefèvre, N., Smythe, T., Hartman, S., Reverdin, G., Gonzalez-Davila, M. & Fietzek, P. (2018). Deliverable D2.4: SOOP Network Enhancement Report, AtlantOS – 633211 project.

Weiss, R., 1974. Carbon dioxide in water and seawater: the solubility of a non-ideal gas. Marine Chemistry, 2 (3): 203-215.

Wimart-Rousseau, C., Fourrier, M., Fiedler, B., Cancouet, R., Claustre, H. and Coppola, L. (2022): development of BGC-Argo data quality validation based on an integrative multiplatform approach. EuroSea Delivrable, D7.2. EuroSea, 29pp. https://doi.org/10.3289/eurosea_d7.2.

Woosley, R. J., F. J. Millero, and R. Wanninkhof (2016), Rapid anthropogenic changes in CO_2 and pH in the Atlantic Ocean: 2003–2014, Global Biogeochem. Cycles, 30, 70–90, doi:10.1002/2015GB005248.

Zhong, G., Li, X., Song, J., Qu, B., Wang, F., Wang, Y., et al. (2022). Reconstruction of global surface ocean CO2 using region-specific predictors based on a stepwise FFNN regression algorithm. Biogeosciences, 19(3), 845–859. https://doi.org/10.5194/bg-19-845-2022

Zhong, G. (2021). Global surface ocean pCO2 product based on a stepwise FFNN algorithm. Marine Science Data Center of the Chinese Academy of Sciences (Http://Msdc.Qdio.Ac.Cn). Dataset. https://doi.org/10.12157/iocas.2021.0022

Supplementary Material

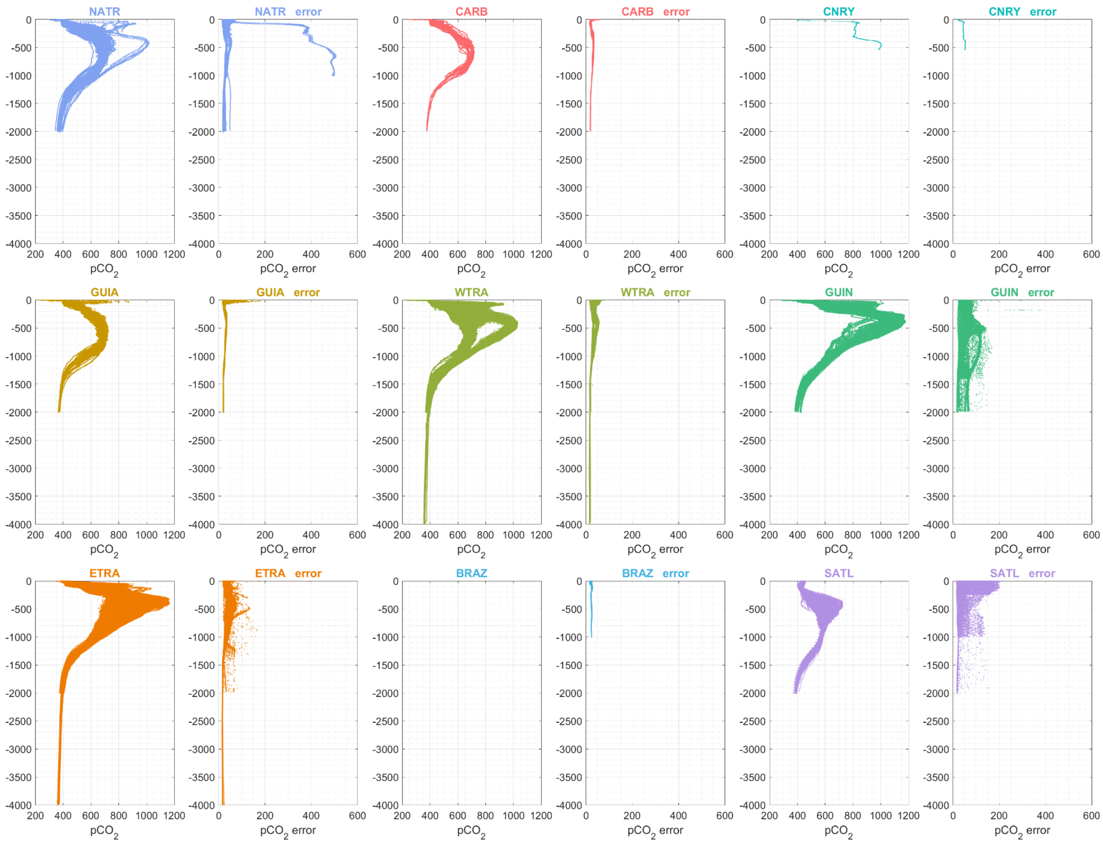

Supplementary Figure 1. Neural network-derived pCO2sw (CONTENT) and associated error over the vertical for each BGCP.

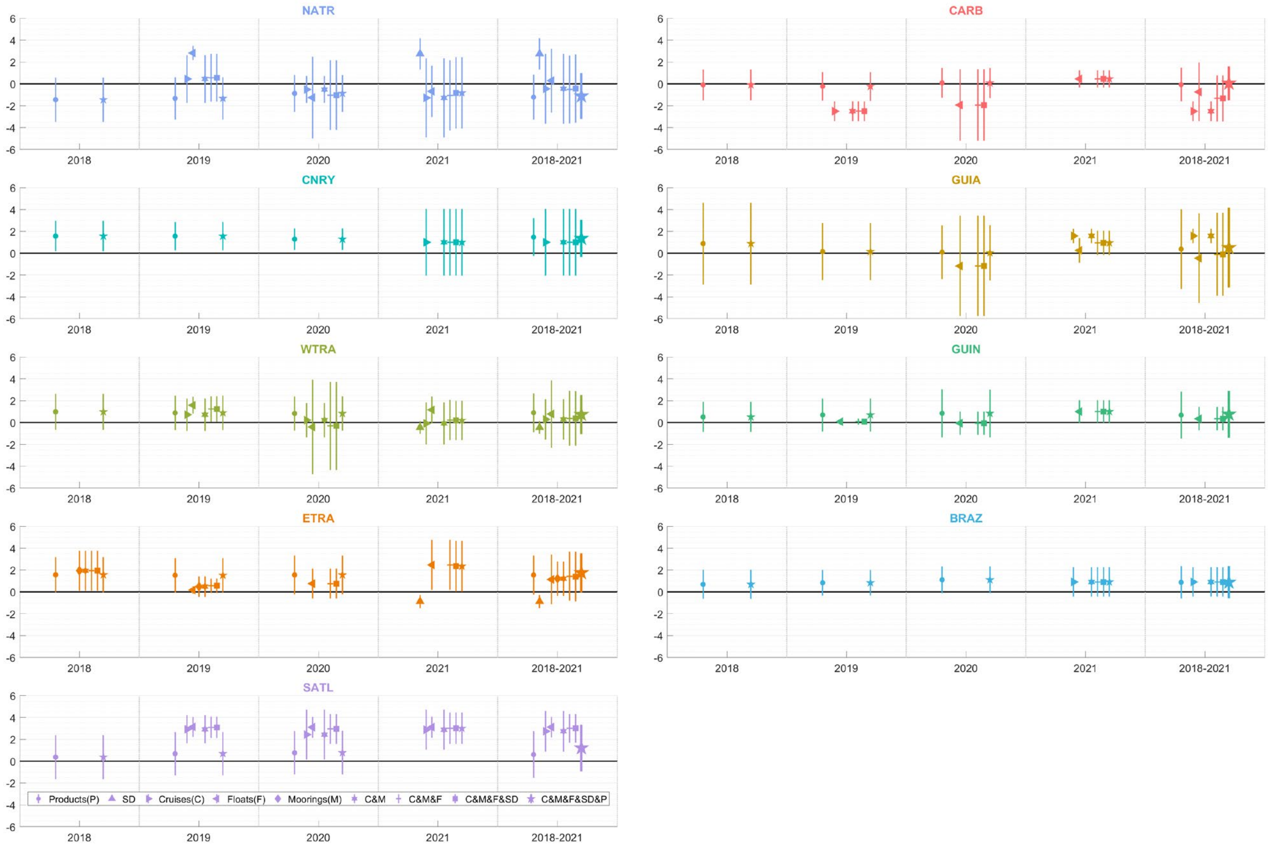

Supplementary Figure 2. FCO2 (mmol.m-2.d-1) averages per year and over the 2018-2021 period per BGCP. Different estimates are provided for each period and area using a different mix of platforms: products (dot), Saildrone (upward triangle), cruises (right-facing triangle), floats (left-facing triangle), moorings (diamond), cruises and moorings (cross), cruises and moorings and floats (plus sign), cruises and moorings and floats and saildrone (square), cruises and moorings and floats and saildrone and products (pentagram). For each individual, the mean ± standard deviation in the area is shown whereas, for the right panels 2018-2021, the mean ± standard deviation of all platforms is shown.

Supplementary Text 1

Using each observing platform and model, the average FCO_2 per year and area were calculated. Furthermore, different mixes of platforms were also used to calculate these fluxes (Supplementary Figure 2). The fluxes for each year from 2018 to 2021 were averaged. Overall, the NATR and CARB are CO_2 sinks over 2018-2021 whereas SATL, ETRA, and BRAZ are net sources. The WTRA, CNRY, GUIN, and GUIA BGCPS are close to zero exhibiting no distinct sink or source behavior. The large discrepancies in coverage and values between the different platforms might bias the overall results. For example, Saildrone estimates in the ETRA BGCPs were significantly lower than the other platforms, qualifying the area as a sink whereas it appears to be a source of CO_2 and the opposite is true for Saildrone-based estimates in the NATR.

Therefore, while providing high-accuracy local estimates of pCO_2 and consequently of FCO_2, Saildrone data cannot be used to extrapolate global behavior over a larger area. In our case, the SD measurements were restricted to one season which might explain the mismatch with the other estimates. Furthermore, these types of platforms might not be the most cost-effective way to obtain CO_2 measurements. Float-based estimates have larger uncertainties than any of the other platforms, but can be used to densify measurements and strengthen area-wide estimates.

Estimates over the 2018-2021 period from all measurement platforms were integrated over the area of each BGCP in an attempt to provide an overall FCO_2 value leaning towards a sink or source of CO_2 to the atmosphere.

Supplementary Table 1: FCO_2 ($mmol.m^{-2}.d^{-1}$) averages over the 2018-2021 period per BGCP, surface of the BGCP, and area integrated FCO_2 estimate ($mmol.y^{-1}$).

Supplementary Table 1. FCO2 (mmol.m-2.d-1) averages over the 2018-2021 period per BGCP, surface of the BGCP, and area integrated FCO2 estimate (mmol.y-1).

	NATR	**CARB**	**CNRY**	**GUIA**	**WTRA**	**GUIN**	**ETRA**	**BRAZ**	**SATL**	**TOTAL**
2018-2021 estimate (mmol/m²/d)	-1.115	0.058	1.355	0.506	0.726	0.762	1.744	0.881	1.210	6.126
Surface (*10³ km²)	8,200	4,396	750	1,236	5,348	1,347	5,323	1,220	17,738	45,559
2018-2021 area integrated estimate (mmol/y)	-25.053	0.698	2.786	1.713	10.638	2.813	25.432	2.942	58.815	80.784